Received: 21 May 2021, Accepted: 12 August 2021, Published: 30 November 2021, Publisher: UTP Press, Creative Commons: CC BY-NC-ND 4.0

EFFECT OF CALCINATION TEMPERATURE ON ELECTROMAGNETIC PROPERTIES OF SANDSTONE SATURATED WITH BFO FOR ENHANCED OIL RECOVERY (EOR) APPLICATION

Alex Teh Boon Li*, Hassan Soleimani, Jemilat Yetunde Yusuf, Lee Kean Chuan

[1]Department of Fundamental and Applied Sciences, Universiti Teknologi PETRONAS, Malaysia

*Email: alex_17000577@utp.edu.my

ABSTRACT

In this paper, BFO NPs were synthesized to prepare nanofluid using the nitric-assisted sol-gel method followed by calcination at different temperatures 200, 350, 500, and 650°C. Sandstone samples were then saturated with as-prepared nanofluids for electromagnetic properties measurements. The effect of calcination temperature on the structural and morphological aspect of BFO NPs was studied using XRD and FESEM. The electromagnetic absorption of the saturated sandstones was measured using the vector network analyzer at X band frequency. The measured scattering parameters were validated with simulation using the finite element method. The simulation results showed that the maximum absorption from the simulation for each sample are 5.73, 5.93, 36.60, 33.19, 36.13dB for S_{brine}, S_{200}, S_{350}, S_{500}, S_{650}, respectively. On the other hand, experimental results showed that the maximum absorption for S_{brine}, S_{200}, S_{350}, S_{500}, and S_{650} is 51.93, 11.63, 8.98, 7.79, 6.97dB, respectively. BFO NPs calcinated at 650°C have the best permittivity values of 10.08 and 3.27 and have the highest real permeability value of 1.22 compared to other samples. Conclusively, the BFO nanoparticle calcinated at 650°C shows the best potential for enhanced oil recovery, which can be selected for further study for EOR application.

Keywords: *Nanofluid, porous rock, calcination, microwave absorption, $BiFeO_3$ NPs, sol-gel*

INTRODUCTION

Ever since the discovery of oil as a source of energy globally , the energy demand has become ever-increasing on a yearly basis. However, several research efforts have been made towards the development of alternative energy sources e.g., renewable energy, there is still a gap for renewable energy to replace oil and gas entirely [1]. Thus, in order to sustain our society until the time where renewable energy is capable of completely substituted oil and gas as a primary source of energy, it is essential to maximize the production of oil from the existing oil fields [2]. Oil recovery operations are subdivided into three stages: primary, secondary, and tertiary oil recovery methods. According to Ali et al. [3], about 30% to 60% of oil remains in most reservoirs after both primary and secondary recovery. However, the amount of fossil fuels is limited, finite, and it is getting harder to extract them from the same reservoir. Besides, the production rate of the existing fields is declining, and the frequency of new site exploration has also become tremendously low over the past decades [4]. Several recent studies have proposed the use of dielectric NPs with an electromagnetic field for Enhanced Oil Recovery (EOR). However, despite their responsive behaviour as absorbing materials for EOR agents, some problems arise and create questions regarding the efficiency of these particles and EOR mechanisms. Previous studies have reported nanomaterials' dielectric and magnetic properties, such as (ZnO, NiO, or Fe_2O_3) for EM waves absorption for EOR application. However, the existing literature lacks studies on sandstones' dielectric and magnetic properties saturated in multiferroic BFO nanofluid. Multiferroic materials have a unique property, they possess two or more of the primary ferroic ordering

in the same phase. It has been widely used in many applications such as ferromagnetic resonance, sensors, data storage, photocatalyst, spintronic, etc. [5]. Among the other multiferroic materials, $BiFeO_3$ (BFO) is one of the few magnetoelectric materials at room temperature [6]-[7]. The researchers have extensively investigated it due to its interesting ferroelectricity and anti-ferromagnetism properties [8]. Thus, it is widely studied for many potential electronics and other industries applications [9].

In recent years, BFO NPs were reported to be synthesized by several methods such as solid-state [10], auto-combustion [11]-[12], hydrothermal [13]-[14], sol-gel [9],[15]-[17], co-precipitation [5],[18] etc. Metal oxide NPs have interestingly gained much attention due to their attractive thermal, electric, and magnetic properties that showed they are potential candidates for enhanced oil recovery. A novel technique called Electrical Enhanced Oil Recovery (EEOR) was first investigated by Haroun et al. [19] using Fe_2O_3, CuO, and NiO Nanoparticles (NPS). These NPs increased the oil recovery with water-flooding by 9 – 22% in the presence of an electrical field. Besides, Zinc Oxide (ZnO) has been considered as a potential material for EOR due to its excellent dielectric properties and high dielectric loss in the presence of the EM field. ZnO and Al_2O_3 NPs have been studied extensively [4],[20]-[21] due to their fantastic dielectric properties that enable the polarization of the NPS to occur underexposure to an electric field. However,it is shown that dielectric NPs, such as Al_2O_3 and ZnO, improve the ROIP by 10% compared to without the presence of EM wave. According to the polarization model, the electrorheological effect is directly influenced by dielectric loss–the greater the dielectric loss, the strong the electrorheological effect [20]. Some studies also proposed the use of either magnetic nanofluid or dielectric nanofluid to increase oil recovery. For instance, Ferromagnetic NPs $CO^{2+}{}_xFe^{2+}{}_{1-x}Fe^{3+}{}_2O_4$ were being studied by Soleimani, et al. [22], results showed that the sample irradiated by electromagnetic (EM) waves achieved 20% higher residual oil in place (ROIP) compare to the one without any EM radiation at 75MHz [23]. The viscosity and mobility of the oil decreased due to the heating of the oil generated by the rotational and alignment of magnetic NPs when they are subjected to the oscillating magnetic field. In another study, Soleimani et al. [23] synthesized a novel– Yttrium Iron Garnet ($Y_3Fe_5O_{12}$) using the sol-gel method to study its effect in EM-assisted EOR. The core flooding results showed that this nanoparticle yielded the recovery of 43.64% ROIP at 13.6MHz EM waves. Ali, et al. [3], compared the performance of $BiFeO_3$ and ZnO NPs in another study, and it was observed that $BiFeO_3$ performs better as an EOR agent due to its high complex permittivity and permeability compared to ZnO. Aside that, it has a higher reflection loss of –9.77dB at high frequency and also displays higher stability at the X-band frequency. Currently, there are only a few studies on the electromagnetic properties of sandstone [24] or sandstones saturated by various types of nanofluid [3]. To the best of the author's knowledge, there is study has been conducted on relationship between the calcination temperature and the EM absorption of sandstone saturated with BFO nanofluids and brine. Some studies dielectric and magnetic properties of palletized BFO nanopowder, but effect of calcination temperature on the electromagnetic absorption of sandstone saturated with different nanofluids in X-band frequency has not been explored. Thus, here in, the electromagnetic properties of sandstone saturated with BFO was studies at X band frequency for EOR application.

METHODOLOGY

Materials

Bismuth (III) nitrate pentahydrate (99%, Aldrich), iron (III) nitrate nonahydrate (99%, Schmidt), ethylene glycol (1,2-ethanediol), nitric acid (65 wt%, Fisher), sodium chloride (NaCl), and sandstone (Angsi-E2) were used in this study. All chemicals used were analytical grade. Distilled water was used at all stages of the experiment.

Synthesis of $BiFeO_3$ NPs

BFO NPs were synthesized using the nitric-assisted sol-gel method referred from a study [25]. Bismuth (III) nitrate pentahydrate, $Bi(NO_3)_3–5H_2O$) and Iron (III) nitrate nonahydrate ($Fe(NO_3)_3–9H_2O$) were dissolved in a stoichiometric ratio of 1:1 into 80 ml ethylene glycol ($C_2H_6O_2$). In order words, approximately 22.4g of $Bi(NO_3)_3–5H_2O)_3$ and 22.4g of $Fe(NO_3)_3–9H_2O$ were dissolved in 80ml of EG (~88.8g) in order to obtain an EG/NO_3^- of 4 molar ratio. The redox reaction between the NO_3^- anions and the OH group of the EG yielded nitrogen oxides (NO_x) that gave the brownish color to the mixed solution [25]. Glyoxylate ($C_2H_2O_4^{2-}$)

ligands were also produced from the redox reaction, as given by:

$$HO - CH_2 - CH_2 - OH + 2NO_2^- \rightarrow C_2H_2O_4^{2-}) + 2NO + 2H_2O \quad (1)$$

During the redox reaction, the glyoxylate ligands are produced to act as chelating agents for Fe^{3+} and Bi^{3+} cations and form a homogenous polyester precursor without the segregation of the cations [26]. The mixed solution was stirred then for 20 minutes at room temperature until the nitrate salts were completely dissolved. 5 mL of nitric acid was added to act as a catalyst and lower the pH value of the solution down. The resulting solution was then heated at 80°C and stirred continuously for 30 minutes until a dark reddish-brown transparent sol was obtained. The sol was then transferred into 4 Petri dishes and put in the oven to dry for 1hr at 110°C to obtain xerogels. The xerogels of each Petri dish were transferred into crucibles. Each xerogels was then calcinated in the air at 200°C, 350°C, 500°C, and 650°C for 4 hours to remove any volatile matter residues and water molecules. After the calcination process, well-crystallized BFO products were obtained then grounded into powder form using a mortar and pestle. Each powder was labeled according to their calcinated temperature; BFO200, BFO300, BFO500, and BFO650.

Preparation of nanofluid

Nanofluid was prepared using a two-step method whereby 0.1 wt% as-synthesized BFO NPs were dispersed in 3% wt brine to act as dispersion fluid. The resulting solution was magnetically stirred for 1 hr to achieve homogenous dispersion. On the other hand, a brine solution without BFO NPs was prepared with 15 wt% of NaCl as control. The sandstone samples were cut and filed to the size of 0.5 × 1 × 2.3 cm to fit perfectly in the sample holder of the X-band waveguide of the vector network analyzer. The sandstones were then immersed in the prepared nanofluids respectively; Brine, BFO200, BFO300, BFO500, and BFO650.

Table 1 The concentration of salt and NPs for the preparation of sandstone saturated with nanofluid and brine

Sample labelling	Composition	wt% of NaCl	wt% of NPs
S_B	Brine	15	0
S_{200}	Brine, BFO200	3	0.1
S_{350}	Brine, BFO350	3	0.1
S_{500}	Brine, BFO500	3	0.1
S_{650}	Brine, BFO650	3	0.1

Characterization

The crystallinity and phase compositions of the as-synthesized BFO powders calcinated at various temperatures were characterized with powder X-ray diffraction (XRD, Panalytical Xpert3) using monochromatic *Cu Kα* radiation (λ = 1.5406Å) in the diffraction angle (2θ) ranging from 10° to 70°. The data were collected with 0.02° step size. The morphology and particle size of the BFO samples were examined by Field Emission Scanning Electron Microscope (FESEM, Zeiss Supra V55) incorporated with Energy Dispersive X-ray Spectroscopy (EDX). The electromagnetic absorption properties of the saturated sandstones (thickness = 0.5cm) were measured at X-band frequency ranging from 8.2 – 12.4 GHz.using a Vector Network Analyzer (VNA, Keysight E5071C).

Numerical Simulation

In this work, Finite-Element Method (FEM) based numerical simulation with COMSOL Multiphysics software was used to validate the measured properties of the saturated sandstones with VNA. The model was based on a 2 ports rectangular waveguide Transverse Electric (TE10) mode with wave excitation at one end (Port 1) and exit from the other end (Port 2), as shown in Figure 1 [3],[27]. Maxwell's equation is required to describe the EM wave propagation. (4) represents the three-dimensional far-field pattern of a plane wave that is expressed in terms of complex permittivity, permeability, and the conductivity of the medium [3],[27]-[28]:

$$\nabla \times \mu_r^{-1} (\nabla \times E) - k_o^2 \left(\varepsilon_r = \frac{j\sigma}{\omega \varepsilon_o} \right) E \equiv 0 \quad (2)$$

where μ_r is the relative permeability, E is the electric field vector, k_o is the wavenumber in free space, ε_r is the relative permeability, ω is the angular frequency, σ is the conductivity of the medium, ε_0 is the permittivity of free space. In the simulation model, assumptions such as $\sigma = 0$ $\mu r = 1$ have been made to express Equation 1 in terms of refractive index. The relative complex permittivity and relative complex permeability obtained from the VNA analysis were

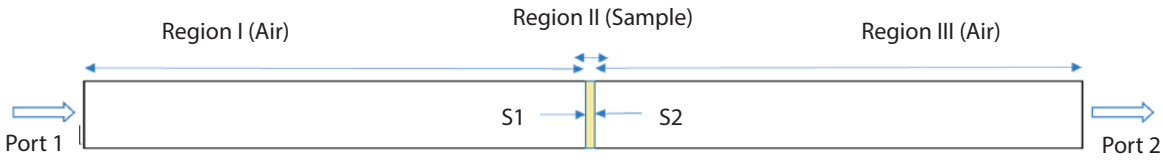

Figure 1 Rectangular waveguide loaded with nanofluid

then used to calculate the refractive index using the formula:

$$Refranctive\ index,\ n = \sqrt{\varepsilon_r \mu_r} \tag{3}$$

A Refractive index is used for the electric displacement model in the simulation. Then, scattering parameter (S) for the incident and transmitted waves in a two-port system, as shown in Figure 2, were calculated to measure the reflection and transmission coefficients during the simulation of sandstone saturated with brine and nanofluids. The scattering parameter for port 1 (S1) and port 2 (S2) can be calculated using the formulas as shown:

$$S_1 = \frac{\int_{port\ 1} ((E - E_1)\cdot E_1) dA_1}{\int_{port\ 1} (E_1 \cdot E_1) dA_1} \tag{4}$$

$$S_1 = \frac{\int_{port\ 2} ((E - E_2)\cdot E_2) dA_2}{\int_{port\ 2} (E_2 \cdot E_1) dA_2} \tag{5}$$

Where E_1 and E_2 are the electric field patterns on ports 1 and 2 separately. The reflection (R) and transmission (T) are related to the scattering parameters by the equations given as:

$$R = |S_1|^2 \tag{6}$$

$$R = |S_2|^2 \tag{7}$$

And that can be used to compute the reflection loss (RL) using the formula:

$$RL = 10\log(1 - R) \tag{8}$$

The simulated result can then be compared with the measured result using VNA from the experiment.

RESULTS AND DISCUSSION

Structural and morphology analysis

The morphology of the BFO calcinated at 350°C appears to have an agglomeration of many small-sized particles. Most of the particles are irregularly shaped microplates with various lengths and widths similar to the morphology of $Bi_2Fe_4O_9$ as reported by Gadhi et al. [29]. This agrees with the high proportion of second phase impurity $Bi_2Fe_4O_9$ in the sample as detected by XRD.

On the other hand, the particles appear to be more angular and anisotropic as the calcination temperature

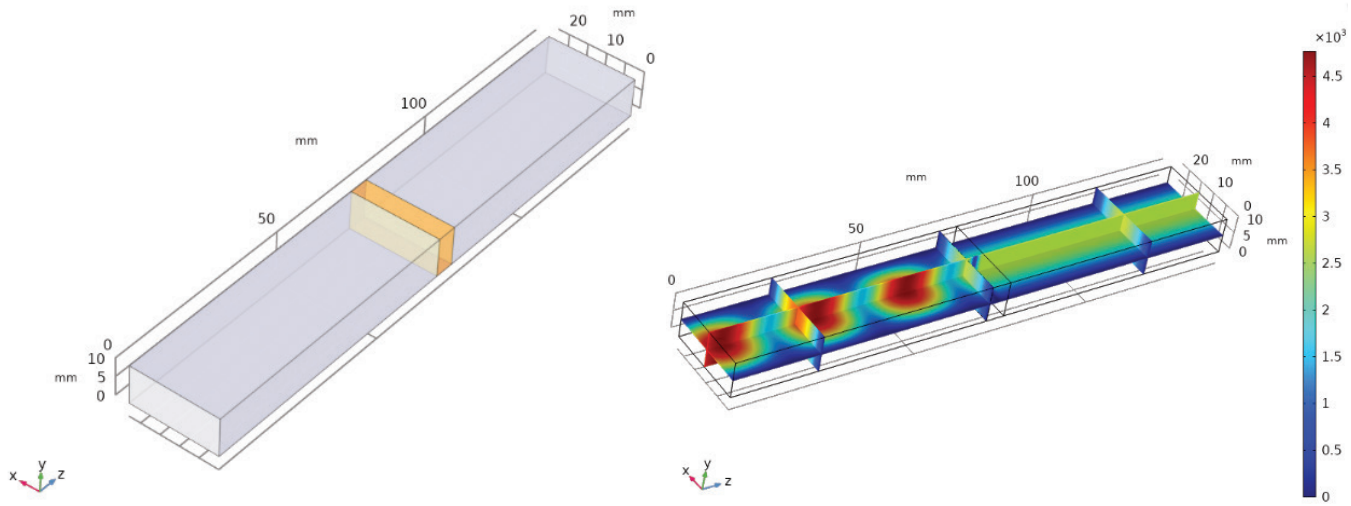

Figure 2 A simulation model and EM radiation pattern across a porous medium with a two-port system

increased to 500°C and 650°C. The BFO NPs calcinated at 650°C are more compact and less porous compared to the rest. Moreover, the grain boundaries appeared to be more visible and larger in BFO NPs calcinated at higher temperatures. The particles appeared to have agglomeration and it is non-homogeneous and decreases as the particle size increases. The agglomeration of particles may be due to the high surface energy of NPs to achieve the most stabilized form, as spherical agglomeration has achieved the lowest surface-to-volume ratio [7]. The average size of the particles for each sample was measured and have been found out to be 94.4, 66.87, 99.69, and 137.53 mm respectively, for BFO (200C), BFO (350C), BFO (500C), and BFO (650C) NPs. The particle size measured by FESEM appeared to be larger than the crystallite size obtained from the XRD because one particle can consist of multiple crystallite domains.

Table 2 EDX weight and atomic ratios of as-synthesized BFO NPs calcinated at 200°C, 350°C, 500°C, and 650°C

Element	Samples	Weight %	Atomic %
Carbon, C	BFO (200C)	24.47	47.34
	BFO (350C)	4.19	15.66
	BFO (500C)	5.73	18.71
	BFO (650C)	9.11	28.29
Oxygen, O	BFO (200C)	31.71	46.07
	BFO (350C)	20.71	58.15
	BFO (500C)	24.05	58.89
	BFO (650C)	15.97	37.23
Iron, Fe	BFO (200C)	5.64	2.35
	BFO (350C)	17.06	13.72
	BFO (500C)	17.98	12.62
	BFO (650C)	43.14	28.81
Bismuth, Bi	BFO (200C)	38.18	4.25
	BFO (350C)	58.05	12.48
	BFO (500C)	52.23	9.79
	BFO (650C)	31.77	5.67

EDX analysis

The Energy Dispersive X-ray Spectroscopy (EDX) analysis was connected to the FESEM spectrometer. The EDX analysis is used to determine the homogeneity and the elemental distribution of synthesized nanocomposite. The weight and atomic ratio of BFO are shown in Table 2 and the EDX spectrum for all the samples are as shown in Figures 3 and 4. It was observed that BFO (500C) has the highest amount of

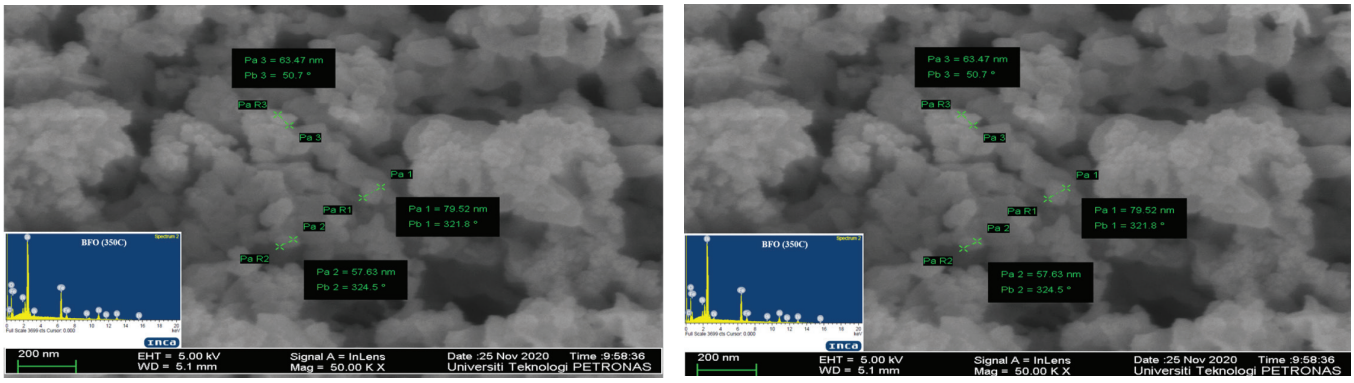

Figure 3 FESEM images of BFO200 and BFO350

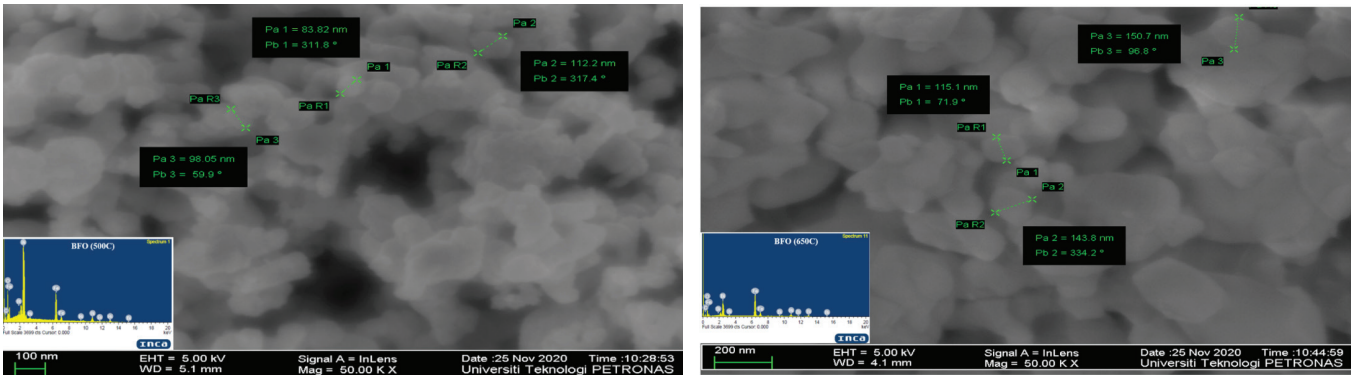

Figure 4 FESEM images of BFO500 and BFO650C at 50.00kx magnification

oxygen (O), BFO (650C) has the highest amount of iron (Fe), and BFO (350C) has the highest amount of Bi. The EDX analysis indicates that the Bi/Fe atomic percent ratio equals 0.196 ~ 0.909, and BFO (350C) has the Bi/Fe ratio closest to 1.0.

XRD analysis

The XRD spectra of BFO NPs calcinated at 200°C, 350°C, 500°C, and 650°C are presented as shown in Figure 5. The XRD spectrum of BFO NPs calcinated at lower temperature BFO (200C) shows the weak characteristic peak, which indicates the amorphous nature of the NPs. However, the XRD pattern for the rest of the BFO NPs calcinated at higher temperatures reveals the presence of more prominent peaks. The secondary impurity phases, such as $Bi_2Fe_4O_9$ and $Bi_{25}FeO_{40}$ were detected at 27.96°, 33.2°, 47°, and 27.4°, 32.19°, 35.68°, 54.2°, respectively. These peaks are denoted by * and ® on the XRD spectra. The similar oxygen affinity of both Bi and Fe ions gives rise to such secondary impurities [30]. The intensity of these peaks decreases as the calcination temperature reaches 500°C and above. The main diffraction peaks of $BiFeO_3$ NPs were observed at 22.45°, 31.77°, 32.08°, 38.94°, 39.49° 45.74°, 51.31°, 51.73°, 66.28°, 67.06° corresponding to (012), (104), (110), (006), (202), (024), (116), (122), (018), (214), (300), (208), and (220) Miller indices, respectively. The splitting of the peak at $2\theta = 32°$ confirms the rhombohedral symmetry of $BiFeO_3$ [31].

The average crystallite size of the as-synthesized nanoparticles was calculated using the Debye-Scherer as given by:

$$D_{XRD} = \frac{k\lambda}{\beta \cos\theta} \tag{9}$$

where $k = 0.9$ is the correction factor, β is the full width at half maximum (FWHM) of the most intense peak, λ is the Cu target wavelength (1.5406 Å) and θ is the glancing angle. The average grain size calculated from the Scherrer equation equals 21.26, 16.41, 30.30 nm for BFO nanoparticles calcinated at 350°C, 500°C and 650°C, respectively. However, an abnormality of higher average crystallite size is observed on the BFO calcinated at 350°C could be associated with the impurity second phase $Bi_2Fe_4O_9$, which is the most intense peak at $2\theta = 27.96°$ in the XRD spectrum.

EM absorption Measurement

The incident EM waves consist of the coupling of an oscillatory E-field and M-field, the material being radiated on will interact with either one of these two

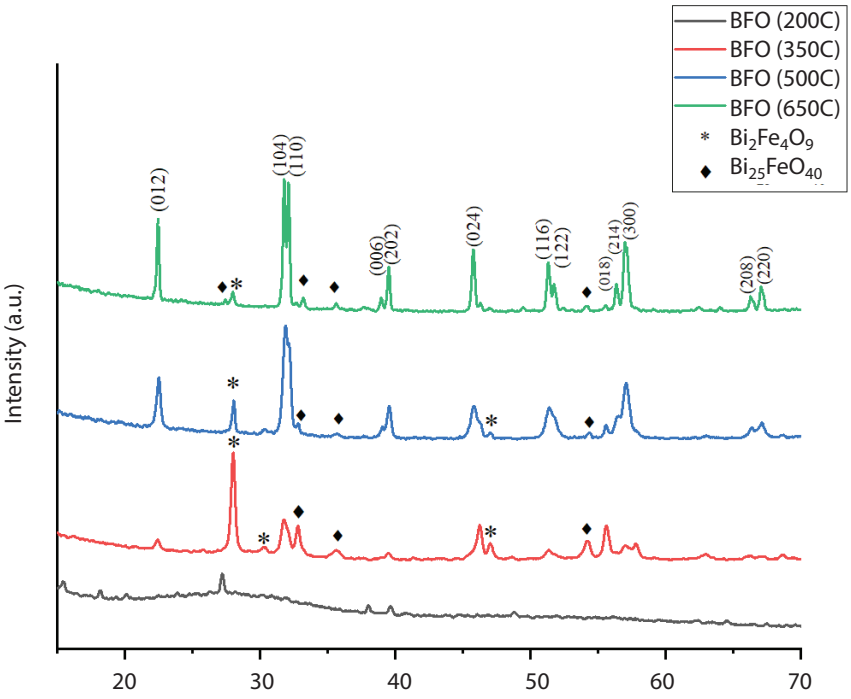

Figure 5 XRD patterns of BFO calcinated at 200°C, 350°C, 500°C and 650°C

fields or both. A multiferroic material such as BFO would respond to both fields simultaneously due to its magneto-electric coupling property [32]. The real part of the permittivity can characterize the amount of energy stored by the material. On the other hand, the conduction current that is caused by the presence of free electrons for conduction represents the imaginary part of permittivity, ε''. The imaginary component represents the total energy loss when radiated by EM waves. The Complex permittivity, ε_r can be expressed as given by:

$$\varepsilon_r = \varepsilon' - j\varepsilon'' \quad (10)$$

where ε' is the real part of the complex permittivity and ε'' is the imaginary part of the complex permittivity. The amount of magnetic loss is represented by the imaginary portion of the complex permeability. The Complex permeability, μ_r is expressed as:

$$\mu_r = \mu' - j\mu'' \quad (11)$$

where μ' is the real part of the complex permeability and μ'' is the imaginary part of the complex permeability. The synthesized bismuth ferrite is susceptible to impurity phases; thus anomalies related to parasitic phases, and defects agglomerated at the grain boundary are expected. Oxygen vacancies are usually present in the samples from mechanochemical synthesis, which leads to valence fluctuation of Fe ions from 3^+ to 2^+ states, resulting in high conductivity in samples. The frequency dependence of real permittivity (ε'), imaginary permittivity (ε'') and dielectric loss (tan δ_ε) of sandstones saturated with brine, and BFO nanofluid calcinated at different temperatures (200°C, 350°C, 500°C, and 650°C) were measured with VNA in X-band frequency (8.2GHz – 12.4GHz) shown in Figure 6. The performance in dielectric properties depends on the ionic, orientational, space charge distribution, etc. [33]. As opposed to the general trend where the real permittivity (or dielectric constant) decreases as the frequency increases. It has been observed that the dielectric constant (ε') remains almost constant throughout the entire range of X-band frequency. This is because, at high frequency, the electric dipoles of the samples failed to keep up and respond to the rapid variation of the alternating applied E-field. The movement of charges became more responsive E-field as the polarization decreases. According to Rhaman et al. [34], this phenomenon is consistent with the Maxwell-Wagner double layer model where the resulted increment in charge movement in neighboring sites is predominated by the characteristics of the the material's dielectric high-frequency region.

Moreover, it can be observed that the value of the dielectric constant (ε') of the sample increases as the calcination temperature increases. Since the dielectric constant (ε'') is directly proportional to the square root of conductivity, the increment in real permittivity appears to imply the decrease in resistivity for the samples, which is in agreement with the work by Ibrahim et al. [35]. According to Rabinkin and Novikova [36] and Khandekar et al. [37], the orientation polarisation of the ferrite materials is mainly due to the presence of the rotational displacement of d Fe^{2+} and Fe^{3+} ions dipoles. In other words, the rotation of Fe^{2+} – Fe^{3+} dipoles can be visualized as the dipoles try to align themselves in response to the alternating E-field by exchanging electrons between one another. Since the perovskites of BFO containing polyvalent cations such as Fe^{2+} and Fe^{3+} are known to exhibit a prominent dielectric permittivity due to electron transfer between both valence states [38], the amount of Fe affects the dielectric properties. The dielectric loss (ε'') showed wide variations with frequency for all the samples. However, dielectric loss is observed as the same trend as the dielectric constant, where it increases as the calcination temperature increases. From both results for dielectric constant and dielectric loss, it is obvious that with the addition of BFO NPs, the dielectric properties of the sandstone saturated with the nanofluid increased. Out of all the samples, the sandstones saturated with BFO nanofluid with calcination temperature of 650°C, S_{650} appears to have the highest dielectric loss in the range of 10-11 GHz. The average value of ε'' for S_{500} and S_{650} are 2.18 and 3.27, higher than the rest of the samples.

As mentioned earlier, multiferroic NPs are capable of displacing oil with the same mechanism as the electrorheological fluids (ERF), and the electrorheological (ER) effect is heavily dependent on the dielectric loss. The greater the dielectric loss, the stronger the ER effect [20]. S_{650} appears to be the best candidate for EOR application as it has the best dielectric properties amongst the others. The ratio of

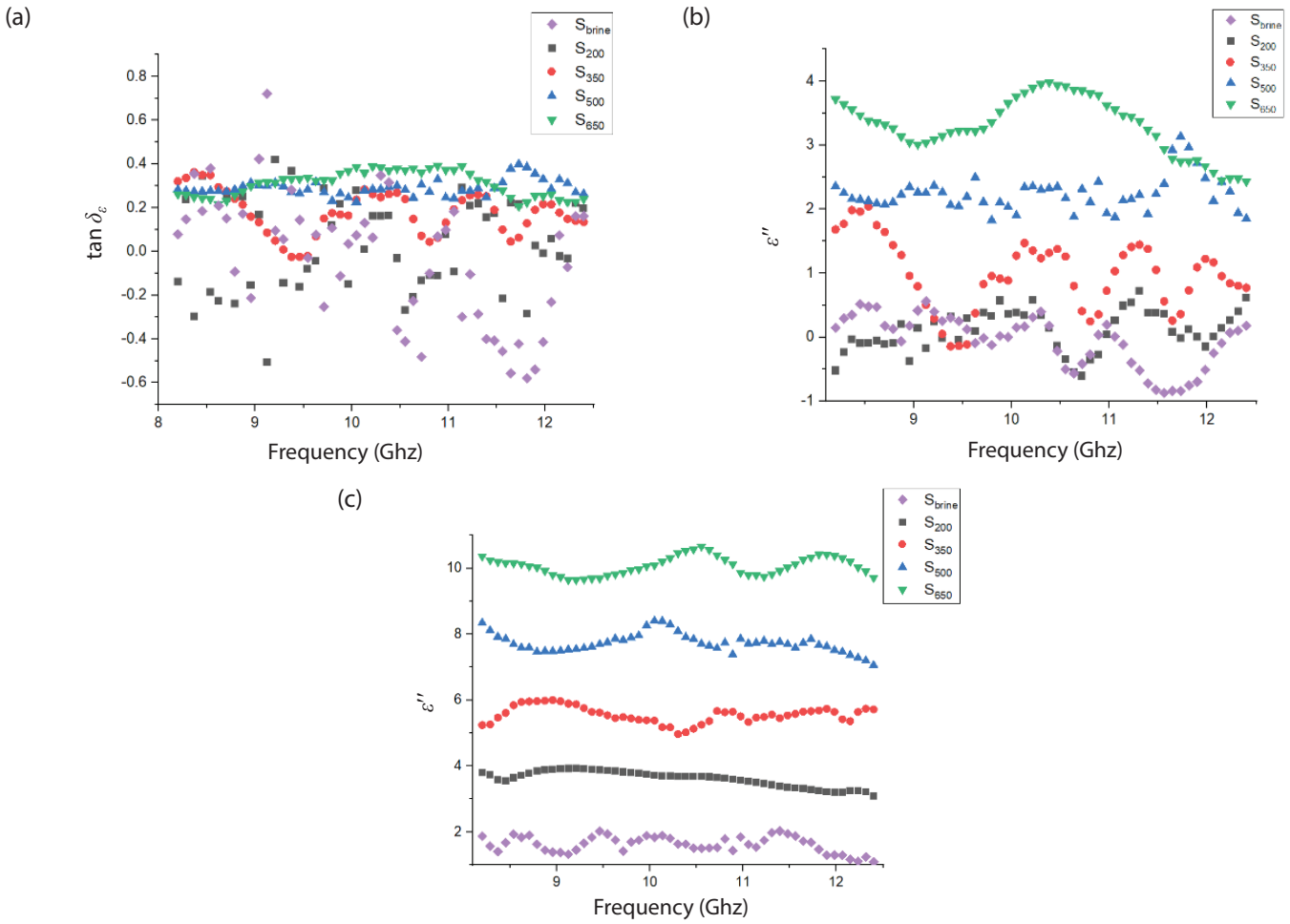

Figure 6 (a) The behavior of dielectric permittivity (ε') as a function of frequency for S_{brine}, S_{200}, S_{350}, S_{500}, S_{650} (b) dielectric loss(ε'') (c) dielectric loss (tan δε).

dielectric loss (ε') with respect to dielectric constant (ε'') can be referred to as dielectric loss factor (tan δ_ε), expressed as:

$$\tan \delta_\varepsilon = \frac{\varepsilon''}{\varepsilon'} \quad (12)$$

where δ_ε is the loss angle between the two components. Similar to its magnetic counterpart, magnetic loss factor (tan δ_μ) can be expressed as the ratio of magnetic loss (μ'') with respect to permeability (μ') as shown:

$$\tan \delta_\mu = \frac{\mu''}{\mu'} \quad (13)$$

where is the loss angle between the two components.

Generally, the loss factors can be used to quantify the effect of energy loss in a lossy material, in this case, it can be due to domain wall resonance due to the high-frequency range. Based on Figure 6, the dielectric loss factor of S_{350} appears to be higher in the range of 8.2-8.5 GHz. Whereas S_{650} has the broadest range of dielectric loss values from around 8.6 GHz to 11.3 GHz, and the value decreases afterward.

The magnetic properties, such as permeability, magnetic loss, and magnetic loss factor, are plotted against the X-band frequency, as shown in Figure 7. The value of μ' and μ' are generally smaller in magnitude compared to dielectric properties, and the μ' does not vary much as the frequency increases. However, the magnetic performance appears to improve as the calcination increases. The average value of μ' increases from as low as around 0.4 by S_{brine} to the highest value around 1.3 by S_{650}. It is also observed that adding BFO nanofluid improves the magnetic performance of the sandstone. As the calcination temperature increases, the crystalline size increases. Increasing

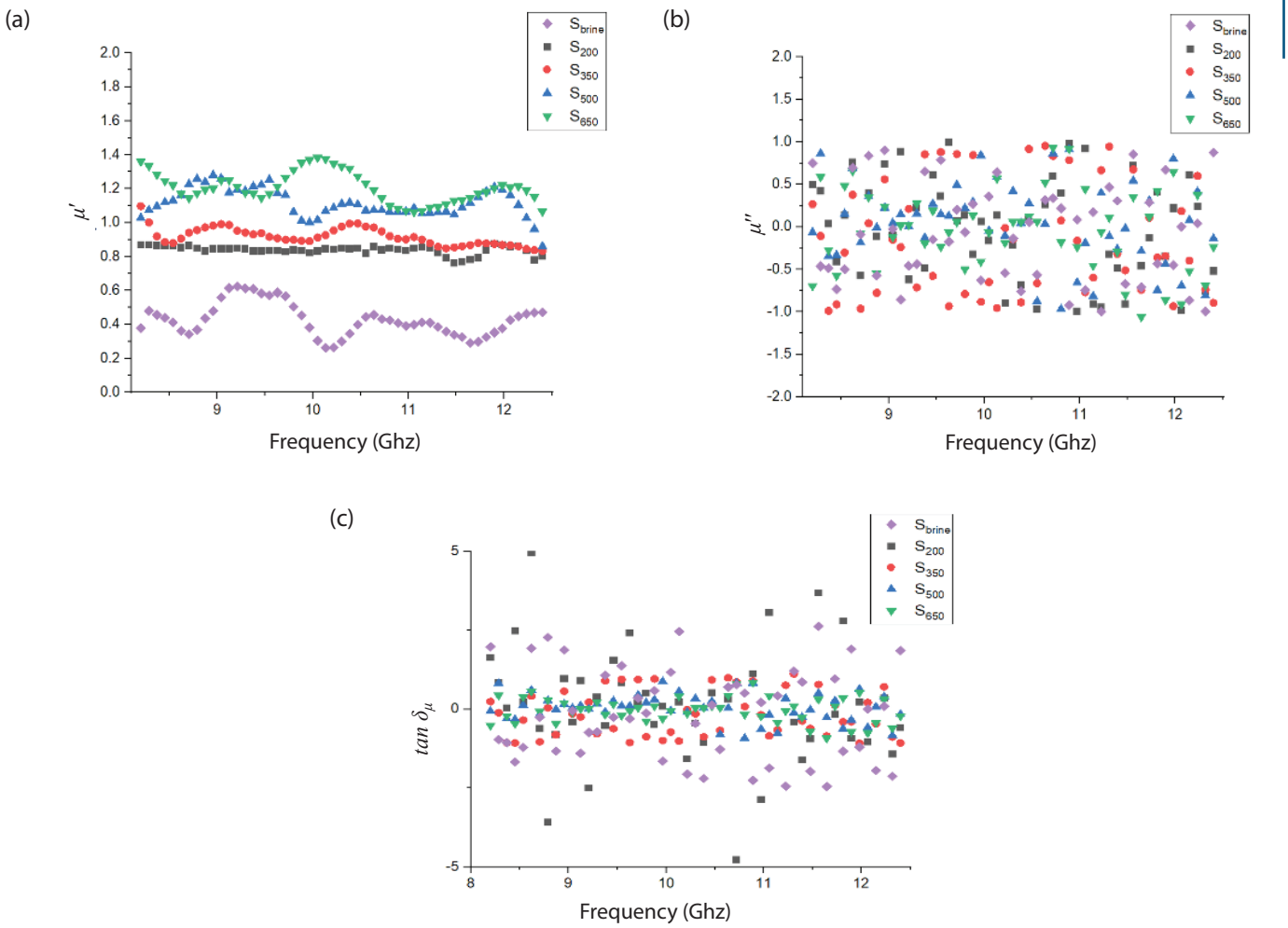

Figure 7 The graph of (a) The behavior of permeability (μ') in X-band frequency range for S_{brine}, S_{200}, S_{350}, S_{500}, and S_{650} (b) magnetic loss (μ'') (c) magnetic loss factor (tan δ_μ)

crystal size is expected to decrease coercivity due to the grain boundaries at which the domain walls are pinned decreases. Since pinning sites are the main source of coercivity, decreasing the size of pinning size decreases coercivity which means increases in permeability [35].

According to recent studies, the presence of oxygen (O) defects that lead to Fe^{2+} ions and grow of magnetic Fe2O3 as an impurity are the source of magnetization of BFO. Since the average crystalline size of the as-synthesized BFO NPs is small on average (d << 65nm), therefore they exhibit stronger multiferroic properties. The cycloid structure of BFO NPs is being suppressed with smaller crystalline size, which enhances the magnetic moments [30],[39]. For the μ'', the data obtained for all samples dispersed within the range of 1.0 and –1.0. The negative values of μ'' observed indicate the transformation from magnetic to electrical energy. Thus, S500 and S650 have the highest average value of μ'' (0.042 and 0.089) compared to the other samples. Although magnetic loss factor (tan δ_μ) values presented in Figure 7 shows a huge variation for all samples, the tan δ_μ appears smaller compared to the tan δ_ε. This matches the experimental results from Ali et.al and Reshi et al. [3],[33], suggesting that dielectric loss is the major contributor in EM radiation absorption at X-band frequency.

Reflection loss measurement

According to the microwave absorption theory, the impedance and reflection loss at the X-band frequency band can be calculated using:

$$Z_{in} = \sqrt{\frac{\mu}{\varepsilon}} \tan h\left(j\frac{2\pi ft}{c}\right) \quad (14)$$

$$RL = 20 \log \left(\frac{z_{in} - 1}{z_{in} + 1} \right) \quad (15)$$

where,
Z_{in} = input impedance on the surface
μ = relative permeability
ε = relative permittivity
RL = reflection loss (dB)
j = complex number
f = frequency
c = speed of light
t = thickness of samples used

Based on the formula, the reflection loss (*RL*) is closely related to both complex relative permittivity (ε) and complex relative permeability (μ). In general, any frequency range at which the *RL* is smaller than –10dB is considered effective absorption bandwidth as it corresponds to 90% of EM wave absorption [40]. Figure 8 shows the experimental *RL* curves for all samples ranging from 8.20 GHz to 12.40 GHz. For the calculated data, it can be observed that all of the sandstone samples that are saturated with BFO nanofluid have a reflection loss higher than –10dB with 5mm of thickness. The lowest value of RL calculated is –51.90 dB at 11.40 GHz by S_{brine}.The comparison between numerical simulation and experimental *RL* for all the sandstone samples are shownin Figure 9.

It appears that in the simulated data, the maximum EM adsorption band range is shifted towards the lower portion of the X-band frequency as the calcination temperature increases. S_{350} has a very high reflection in the range of 11.4 – 12.4 GHz, 9.4 – 10.4 GHz for S_{500}, and 8.2 – 8.5 GHz for S_{650}. However, both S_{brine} and S_{200} appear not to have any RL less than -10dB but show a decreasing trend in RL as the frequency increases. The maximum absorption from the simulation for each sample is 5.73, 5.93, 36.60, 33.19, 36.13 for S_{brine}, S_{200}, S_{350}, S_{500}, S_{650}, respectively. The experimental RL for all samples are as shown in Figure 8. The data from the experiment shows a very wavy plot, this may be due to the attenuation of the signal during the measurement of electromagnetic properties. It can be seen that the reflection loss of all the sandstone samples saturated with BFO nanofluid does not reach more than 10dB. And the maximum absorption of the samples appears to have a decreasing trend as the calcination temperature increases. The maximum absorption is 51.93, 11.63, 8.98, 7.79, 6.97 for S_{brine}, S_{200}, S_{350}, S_{500}, and S_{650} respectively. In contrast to the simulated results, no reflection loss response shows minimum value in a range of frequencies. And the absorption performance appears to have no drastic change as the frequency increaseswhich is not in agreement with the simulated results as the errors are not being taken into account in the simulation.

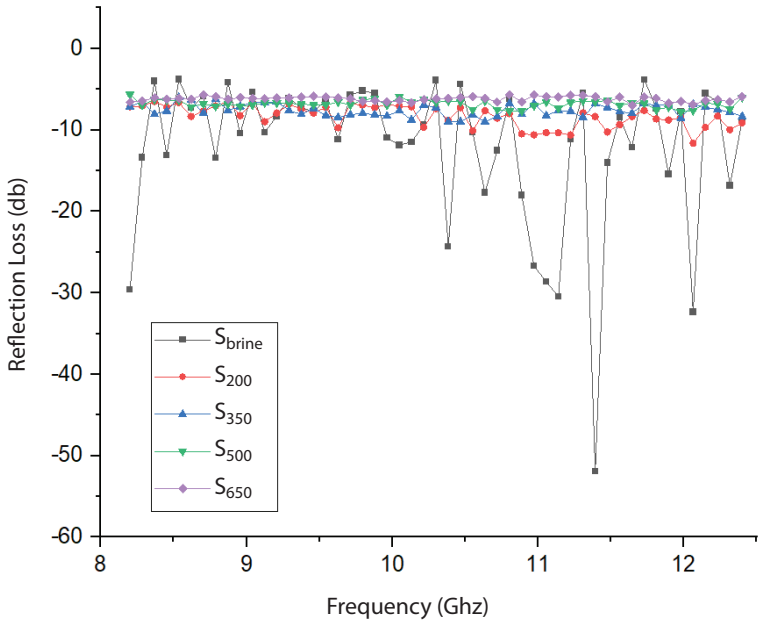

Figure 8 Experimental calculated of Reflection Loss (RL) curve for S_{brine}, S_{200}, S_{350}, S_{500}, and S_{650} at X-band (8.2 GHz – 12.4 GHz) frequency

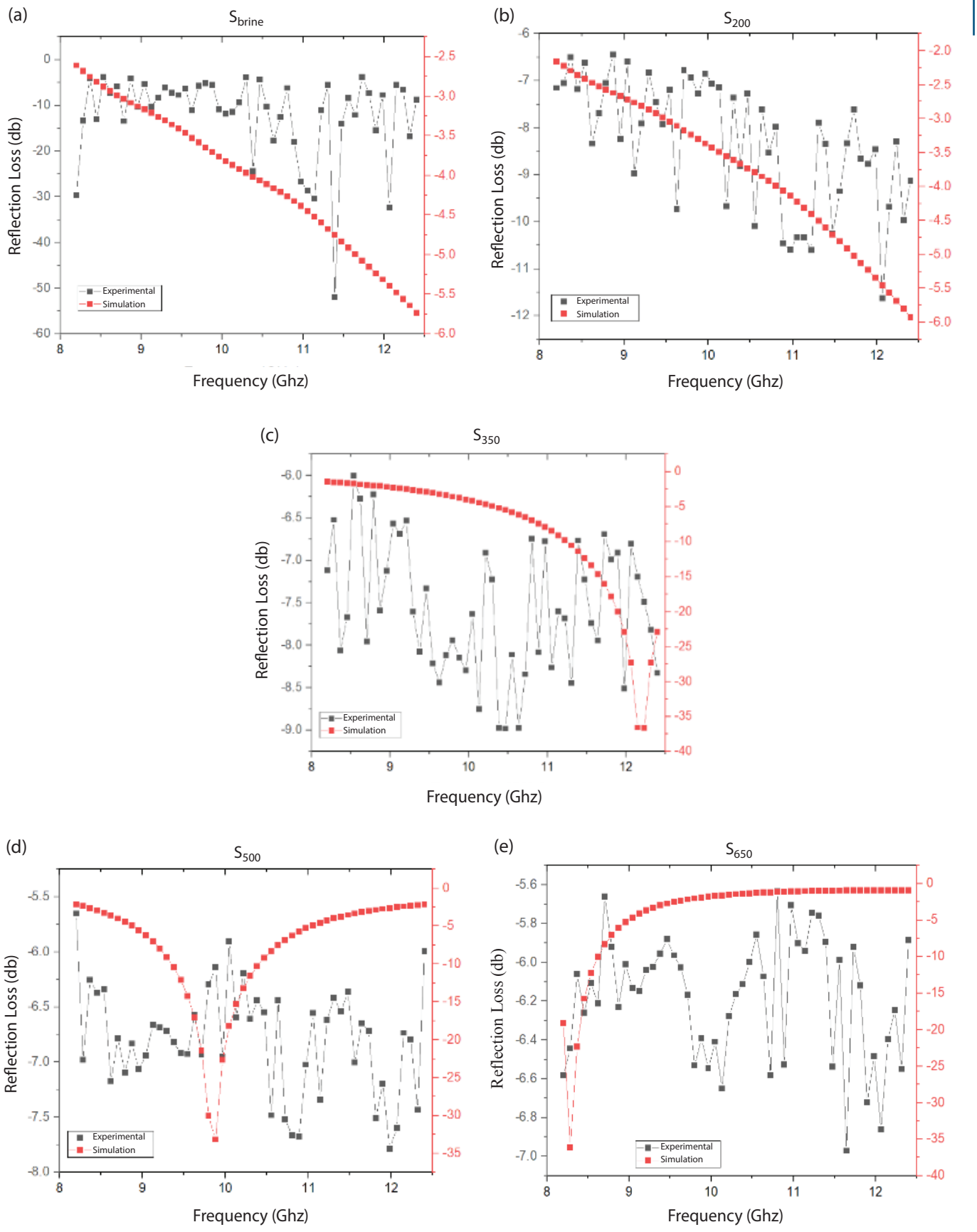

Figure 9 Comparison of the experimental and simulation results for Reflection Loss (RL) (a) S_{brine}, (b) S_{200}, (c) S_{350}, (d) S_{500} and (e) S_{650} at X-band frequency range

CONCLUSION

In conclusion, bismuth ferrite NPs (BFO) were synthesized successfully by using nitric acid-assisted sol-gel using ethylene glycol as solvent. Both the EDX and XRD results confirmed the presence of single-phase bismuth ferrite ($BiFeO_3$) in the samples as the calcination temperature increases with the reduction in impurity phases. The optimum temperature to obtain high purity BFO NPs is 650°C which agrees with many studies in the past. The structural analysis showed the rhombohedral phase formation with crystallite size varying from 18 – 30nm, which showed the trend of increment as the calcination temperature increases once the impurity phases are eliminated. Among all the samples, BFO NPs calcinated at 650°C appear to have the best permittivity values of 10.08 and 3.27 for its real and imaginary counterparts.

Moreover, BFO (650°C) also appears to have the highest real permeability value of 1.22 compared to other samples, although the difference between the samples is very small. It is suggested that to synthesize the BFO NPs with optimum electromagnetic properties for EOR application, the calcination temperature for BFO NPs is set to 650°C. The simulation results on FEM may not seem to agree with the experimental data, which may be due to the assumption made in the simulation that the conductivity and relative complex permeability of the samples are zero. Based on the past experimental study, the network analyzer results showed a similar pattern for sandstone soak with nanofluid. Although the results showed that BFO calcinated at 650°C has the highest potential amongst the other as an EOR agent, it is not very well studied that if the performance of BFO NPs is going to be better in an actual oil recovery experiment. Therefore, it is highly recommended to study the comparison of the performance as an EOR agent between the metal oxide NPs and BFO NPs in a core flooding experiment. All in all, the BFO NPs show great potential as an EOR agent.

REFERENCE

[1] C. Zou, Q. Zhao, G. Zhang, & B. Xiong, "Energy revolution: From a fossil energy era to a new energy era", *Natural Gas Industry B,* 3, 1, pp. 1-11, 2016, doi: https://doi.org/10.1016/j.ngib.2016.02.001.

[2] H. Ali et al., "Enhanced oil recovery by using electromagnetic-assisted nanofluids: A review", *Journal of Molecular Liquids,* 309, p. 113095, 2020, doi: https://doi.org/10.1016/j.molliq.2020.113095.

[3] H. Ali et al., "Absorption of electromagnetic waves in sandstone saturated with brine and nanofluids for application in enhanced oil recovery", *Journal of Taibah University for Science,* 14, 1, pp. 217-226, 2020, doi: 10.1080/16583655.2020.1718467.

[4] H. M. Zaid, N. R. A. Latiff, N. Yahya, H. Soleimani, & A. Shafie, "Application of Electromagnetic Waves and Dielectric Nanoparticles in Enhanced Oil Recovery" *Journal of Nano Research,* 26, pp. 135-142, 2013, doi: 10.4028/www.scientific.net/JNanoR.26.135.

[5] H. Maleki, M. Haselpour, & R. Fathi, "The effect of calcination conditions on structural and magnetic behavior of bismuth ferrite synthesized by co-precipitation method", *Journal of Materials Science: Materials in Electronics,* 29, 5, pp. 4320-326, 2017, doi: 10.1007/s10854-017-8379-z.

[6] D. Carranza-Celis et al., "Control of Multiferroic properties in BiFeO3 nanoparticles", *Science Reports,* 9, 1, p. 3182, 2019, doi: 10.1038/s41598-019-39517-3.

[7] M. Sakar, S. Balakumar, P. Saravanan, & S. N. Jaisankar, "Annealing temperature mediated physical properties of bismuth ferrite (BiFeO3) nanostructures synthesized by a novel wet chemical method", *Materials Research Bulletin,* 48, 8, pp. 2878-885, 2013, doi: 10.1016/j.materresbull.2013.04.008.

[8] N. A. Spaldin, S.-W. Cheong, & R. Ramesh, "Multiferroics: Past, present, and future", *Physics Today,* 63, 10, pp. 38-43, 2010, doi: 10.1063/1.3502547.

[9] J.-H. Xu, H. Ke, D.-C. Jia, W. Wang, & Y. Zhou, "Low-temperature synthesis of BiFeO3 nanopowders via a sol–gel method", *Journal of Alloys and Compounds,* 472, 1-2, pp. 473-477, 2009, doi: 10.1016/j.jallcom.2008.04.090.

[10] D. Maurya, H. Thota, K. S. Nalwa, & A. Garg, "BiFeO3 ceramics synthesized by mechanical activation assisted versus conventional solid-state-reaction process: A comparative study", *Journal of Alloys and Compounds,* 477, 1-2, pp. 780-784, 2009, doi: https://doi.org/10.1016/j.jallcom.2008.10.155.

[11] J.-B. Li, G. H. Rao, J. K. Liang, Y. H. Liu, J. Luo, & J. R. Chen, "Magnetic properties of Bi(Fe1−xCrx)O3 synthesized

by a combustion method" *Applied Physics Letters,* 90, 16, p. 162513, 2007, doi: 10.1063/1.2720349.

[12] S. Vijayanand, H. S. Potdar, & P. A. Joy, "Origin of high room temperature ferromagnetic moment of nanocrystalline multiferroic BiFeO3," *Applied Physics Letters,* 94, 18, p. 182507, 2009, doi: 10.1063/1.3132586.

[13] C. M. Cho, J. H. Noh, I.-S. Cho, J.-S. An, K. S. Hong, & J. Y. Kim, "Low-Temperature Hydrothermal Synthesis of Pure BiFeO3 Nanopowders Using Triethanolamine and Their Applications as Visible-Light Photocatalysts" *Journal of the American Ceramic Society,* 91, 11, pp. 3753-755, 2008, doi: https://doi.org/10.1111/j.1551-2916.2008.02689.x.

[14] S. Blessi, S. Vijayalakshmi, & S. Pauline, "Synthesis, Structural and Dielectric Properties of Pure and Ni Substituted Bismuth Ferrite", *Advanced Materials Research,* 938, pp. 140-144, 2014, doi: 10.4028/www.scientific.net/AMR.938.140.

[15] A. Bismibanu, "Preparation and Characterization of Bismuth Ferrite Nanoparticle Using Sol–Gel Method", *International Journal for Research in Applied Science and Engineering Technology,* 6, 4, pp. 1767-770, 2018, doi: 10.22214/ijraset.2018.4299.

[16] I. Journals et al., "Synthesis of Bismuth Ferrite nano particles by sol-gel method and their characterization", 2015.

[17] M.V Shisode, P.P Khirade, DN. Bhoyar, A.R Chavan, K.M. Jadhav, "Sol-Gel synthesis, Structural and magnetic properties of Multiferroic nanoparticles", *International Journal of Advanced Research in Basic and Applied Science,* pp. 110-112, 2017.

[18] M. Muneeswaran, P. Jegatheesan, & N. V. Giridharan, "Synthesis of nanosized BiFeO3powders by co-precipitation method", *Journal of Experimental Nanoscience,* 8, 3, pp. 341-346, 2012, doi: 10.1080/17458080.2012.685954.

[19] M. R. Haroun et al., "Smart Nano-EOR Process for Abu Dhabi Carbonate Reservoirs", Abu Dhabi International Petroleum Conference and Exhibition, Abu Dhabi2012, doi: https://doi.org/10.2118/162386-MS.

[20] M. Adil, H. Mohd Zaid, L. K. Chuan, & N. R. Ahmad Latiff, "Effect of EM propagation medium on electrorheological characteristics of dielectric nanofluids", *Journal of Dispersion Science and Technology,* 38, 4, pp. 570-576, 2016, doi: 10.1080/01932691.2016.1182922.

[21] M. Adil, K. Lee, H. Mohd Zaid, N. R. Ahmad Latiff, & M. S. Alnarabiji, "Experimental study on electromagnetic-assisted ZnO nanofluid flooding for enhanced oil recovery (EOR)", *PLoS One,* 13, 2, p. e0193518, 2018, doi: 10.1371/journal.pone.0193518.

[22] H. Soleimani, N. Yahya, N. R. A. Latiff, H. M. Zaid, B. Demiral, & J. Amighian, " Novel Enhanced Oil Recovery Method Using $Co^{2+}_{x}Fe^{2+}_{1-x}Fe^{3+}_{2}O_4$ as Magnetic Nanoparticles Activated by Electromagnetic Waves", *Journal of Nano Research,* 26, pp. 111-116, 2013, doi: 10.4028/www.scientific.net/JNanoR.26.111

[23] H. Soleimani et al., "Synthesis and Characterization of Yttrium Iron Garnet (YIG) Nanoparticles Activated by Electromagnetic Wave in Enhanced Oil Recovery", *Journal of Nano Research,* 38, pp. 40-46, 2016, doi: 10.4028/www.scientific.net/JNanoR.38.40.

[24] F. A. Wahaab, L. L. Adebayo, A. M. Ali, & A. O. Yusuff, "Experimental investigation of resonant frequency of sandstone saturated with magnetite nanofluid", *Journal of Taibah University for Science,* 14, 1, pp. 1243-250, 2020, doi: 10.1080/16583655.2020.1816370.

[25] S. Shabani, S. M. Mirkazemi, S. M. Masoudpanah, & P. T. Dolat Abadi, "Synthesis and Characterization of Pure Single Phase BiFeO3 Nanoparticles by the Glyoxylate Precursor Method" *Journal of Superconductivity and Novel Magnetism,* 27, 12, pp. 2795-2801, 2014, doi: 10.1007/s10948-014-2713-y.

[26] S. M. Masoudpanah, S. M. Mirkazemi, S. Shabani, & P. T. Dolat Abadi, "The effect of the ethylene glycol to metal nitrate molar ratio on the phase evolution, morphology and magnetic properties of single phase BiFeO3 nanoparticles," *Ceramics International,* 41, 8, pp. 9642-646, 2015, doi: 10.1016/j.ceramint.2015.04.029.

[27] L. L. Adebayo, H. Soleimani, N. Yahya, Z. Abbas, A. T. Ridwan, & F. A. Wahaab, "Investigation of the Broadband Microwave Absorption of Citric Acid Coated Fe3O4/PVDF Composite Using Finite Element Method", *Applied Sciences,* 9, 18, 2019, doi: 10.3390/app9183877.

[28] F. A. Wahaab, N. Yahya, A.Shafie, H. Soleimani, A. Rostami, & M. Ganeson, "Determination of Optimum Frequency for Electromagnetic-Assisted Nanofluid Core Flooding", *Applied Sciences,* 9, 21, 2019, doi: 10.3390/app9214608.

[29] T. A. Gadhi et al., "Single BiFeO3 and mixed BiFeO3/Fe2O3/Bi2Fe4O9 ferromagnetic photocatalysts for solar light driven water oxidation and dye pollutants degradation", *Journal of Industrial and Engineering Chemistry,* 63, pp. 437-448, 2018, doi: 10.1016/j.jiec.2018.03.004.

[30] H. Singh & J. K. Rajput, "Effect of calcination temperature on magnetic, structural, thermal and optical properties of BFO-T nanoparticles", *SN Applied Sciences,* 2, 8, 2020, doi: 10.1007/s42452-020-3140-2.

[31] J. Wang, Y. Wei, J. Zhang, L. Ji, Y. Huang, & Z. Chen, "Synthesis of pure-phase BiFeO3 nanopowder by nitric acid-assisted gel", *Materials Letters,* 124, pp. 242-244, 2014, doi: 10.1016/j.matlet.2014.03.105.

[32] M. M. Vopson, "Fundamentals of Multiferroic Materials and Their Possible Applications", *Critical Reviews in Solid State and Materials Sciences,* 40, 4, pp. 223-250, 2015/07/04 2015, doi: 10.1080/10408436.2014.992584.

[33] H. A. Reshi, A. P. Singh, S. Pillai, T. A. Para, S. K. Dhawan, & V. Shelke, "X-band frequency response and electromagnetic interference shielding in multiferroic BiFeO3 nanomaterials", *Applied Physics Letters,* 109, 14, 2016, doi: 10.1063/1.4964383.

[34] M. Rhaman, M. Matin, M. Hakim, & M. Islam, "Dielectric, ferroelectric and ferromagnetic properties of samarium doped multiferroic bismuth ferrite" *Materials Research Express,* 6, 12, 2019, doi: 10.1088/2053-1591/ab57c2.

[35] E. M. M. Ibrahim, G. Farghal, M. Khalaf, & H. El-Lateef, "Effect of Calcination Temperature on Magnetic and Electrical Properties of BiFeO 3 Nanoparticles Prepared By Sol-Gel Method", *Advanced Materials,* 5, 1, pp. 33-39, 01/01 2017, doi: 10.18576/jnam/050105.

[36] I. Rabinkin & Z. Novikova, "Ferrites, Izv Acad," *Nauk USSR Minsk,* vol. 146, 1960.

[37] M. S. Khandekar, R. C. Kambale, J. Y. Patil, Y. D. Kolekar, & S. S. Suryavanshi, "Effect of calcination temperature on the structural and electrical properties of cobalt ferrite synthesized by combustion method" *Journal of Alloys and Compounds,* 509, 5, pp. 1861-865, 2011, doi: 10.1016/j.jallcom.2010.10.073.

[38] E. Markiewicz, B. Hilczer, M. Błaszyk, A. Pietraszko, & E. Talik, "Dielectric properties of BiFeO3 ceramics obtained from mechanochemically synthesized nanopowders," *Journal of Electroceramics,* 27, 3-4, pp. 154-161, 2011, doi: 10.1007/s10832-011-9660-9.

[39] A. Manzoor, A. M. Afzal, M. Umair, A. Ali, M. Rizwan, & M. Z. Yaqoob, "Synthesis and characterization of Bismuth ferrite (BiFeO3) nanoparticles by solution evaporation method", *Journal of Magnetism and Magnetic Materials,* 393, pp. 269-272, 2015/11/01/ 2015, doi: https://doi.org/10.1016/j.jmmm.2015.05.066.

[40] B. Zhao et al., "Recent Advances on the Electromagnetic Wave Absorption Properties of Ni Based Materials", *Engineered Science,* 2018, 3, 28, doi: 10.30919/es8d735.